Anti-icing property of bio-inspired micro-structure superhydrophobic surfaces and heat transfer model

Yan Liu[a1], Xinlin Li[a], Jingfu Jin[b], Jiaan Liu[c], Yuying Yan[d], Zhiwu Han[a], Luquan Ren[a]

a. Key Laboratory of Bionic Engineering (Ministry of Education), Jilin University, Changchun 130022, China; b. College of Biological and Agricultural Engineering, Jilin University, Changchun 130022, PR China; c. Key Laboratory of Automobile Materials (Ministry of Education) and College of Materials Science and Engineering, Jilin University, Changchun, 130022, P. R. China; d. Energy & Sustainability Research Division, Faculty of Engineering, University of Nottingham, UK

Abstract

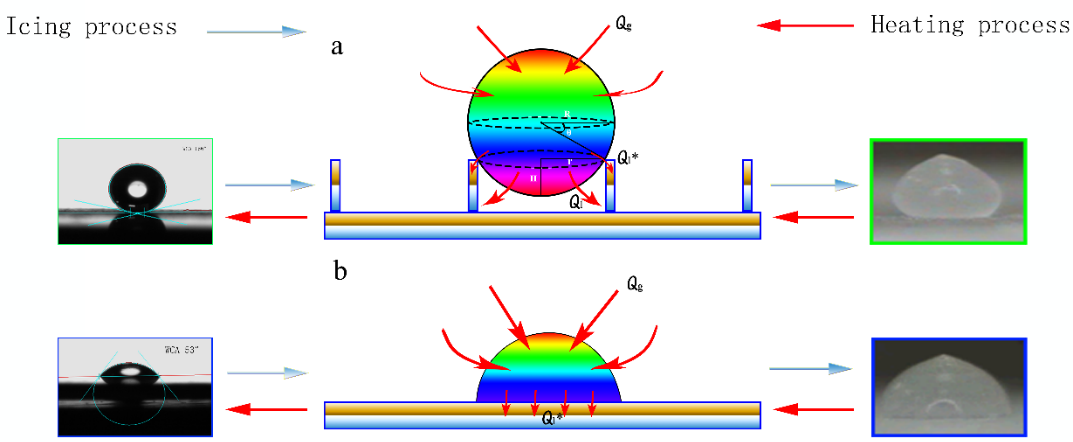

Ice accumulation is a thorny problem which may inflict serious damage even disasters in many areas, such as aircraft, power line maintenance, offshore oil platform and locators of ships. Recent researches have shed light on some promising bio-inspired anti-icing strategies to solve this problem. Inspired by typical plant surfaces with

Corresponding author. Tel.:+86 431 85095760; fax:+86 431 85095575
E-mail address: lyyw@jlu.edu.cn

super-hydrophobic character such as lotus leaves and rose petals, structured superhydrophobic surface are prepared to discuss the anti-icing property. 7075 Al alloy, an extensively used materials in aircrafts and marine vessels, is employed as the substrates. As-prepared surfaces are acquired by laser processing after being modified by stearic acid for 1h at room temperature. The surface morphology, chemical composition and wettability are characterized by means of SEM, XPS, Fourier transform infrared (FTIR) spectroscopy and contact angle measurements. The morphologies of structured as-prepared samples include round hump, square protuberance and mountain-range-like structure, and that the as-prepared structured surfaces shows an excellent superhydrophobic property with a WCA as high as 166 ± 2°. Furthermore, the anti-icing property of as-prepared surfaces was tested by a self-established apparatus, and the crystallization process of a cooling water on the sample was recorded. More importantly, we introduced an model to analyze heat transfer process between the droplet and the structured surfaces. This study offers an insight into understanding the heat transfer process of the superhydrophobic surface, so as to further research about its unique property against ice accumulation.

Key words: Anti-icing, Superhydrophobic, Aluminum alloy, Laser process, Heat transfer

1. Introduction

Many researches for anti-/de-icing performance of the surfaces, such as aircrafts, wind turbines, power lines, marine vessels, highways, buildings, refrigeration equipment, and telecommunication equipment, have been made, because the formation of ice on these surfaces can cause many bad impacts.**[1-3]** Some of the disasters in the aviation, in particular, have been attributed to the accumulation of ice on the windward surface of aircrafts during a flight, for the aerodynamic forces are altered, either increasing drag or decreasing lift. In order to solve this problem, a particular attractive technique, ie. anti-icing performance of SHS (superhydrophobic surface), have been researched recently.**[4-6]**

Inspired by many plants and insects, such as lotus leaves[7], rose petals[8], legs of water striders[9] and butterfly wings[10], wettability[11], which is dominated by both the chemical composition and the morphology of the surface[12, 13], is one of the unusual properties of these plants and insects. Abiding by the mechanism of the wettability[14, 15], the fabrication of SHS involves two steps, the creation of a rough micro/nano scale structure and followed with the passivation of the rough surface by a low surface energy chemical reagents.[16, 17] By now, many studies have successfully fabricated the superhydrophobic surfaces with anti-icing property by various methods. Cao et al.[18] fabricated the superhydrophobic coatings with anti-icing property by using nanoparticle-polymer composites successfully, which are able to prevent ice formation upon impact of supercooled water both in laboratory conditions and in naturally occurring environments, demonstrating that the particle sizes of the coatings are critical for anti-icing property. Guo et al.[19] systematically studied the anti-icing properties of different structured surfaces, i.e. micro/nano- structured surface (MN-surface), nanostructured surfaces (N-surfaces), micro-structured surfaces(M-surfaces), smooth surfaces without any structure (S-surfaces), finding that the MN-surface composed of microratchets combined with nano-hairs on a metal substrate shows an excellent icephobic/anti-icing property than others. Moreover, Kim et al.[20] employed a radically different method to fabricate a new type of ice-repellent material based on slippery, liquid-infused porous surfaces (SLIPS) on aluminum substrates, which is proved to have a promising and broad application for its robust anti-icing properties. Actually, most of researches have proved that morphology of the superhydrophobic surfaces is a very important factor for its anti-icing property.[5, 21-23] And experiments carried out on designed micro-/nanostructured superhydrophobic surfaces show a spontaneous and controllable removal of condensed microdroplets at high supersaturation via self-propelled jumping.[24-27] However, few researches thoroughly elaborate that how the surface morphology influence the heat transfer process.

In this paper, 7075 Al alloy is employed as the substrates of the SHS, which is widely applied in aviation, mechanical equipment, and mould processing, for its excellent property of high strength and mechanical capacity. [28, 29] We study the anti-icing property of SHS on 7075 Al alloy with different morphologies by laser processing, such as round hump, square protuberance and mountain-range-like structure. We demonstrated that the different morphology of the SHS exhibited relatively different anti-icing properties, tested by a robust apparatus established by ourselves, by which we decreased the temperature from the room temperature of 16.0 °C to -15 °C at the rate of 0.2°C/s with the relative humidity of 53±5%, and the icing time on these SHS can be postponed obviously compared to the bare 7075 Al alloy substrate. In order to investigate the anti-icing property in dynamic situations, a stream of water was sprayed on the experimental surfaces after they were tilted, controlling the temperature at -15 °C and the relative humidity of 53±5% stably. Interestingly, the water sprayed on the no structured surfaces iced up and accumulate gradually; while on the SHS flowed down immediately, only small parts of which covered with ice. We find that the anti-icing capability of the SHS, to some extent, is determined by the micro array structure of SHS. Furthermore, we present a model to analyze heat transfer process between the droplet and the structured surfaces.

2. Experimental

2.1 Materials

7075 Al alloy sheets (0.4wt% Si, 0.5wt% Fe, 2.0wt% Cu, 0.3wt% Mn, 2.9wt% Mg, 0.28wt% Cr, 6.1wt% Zn, 0.2wt% Ti, with balance being Al) with the size of 20mm×20mm×1mm, emery paper No. 400, No. 800 and No. 1500, acetone, ethanol and stearic acid ($CH_3(CH_2)_{16}COOH$) (99%, Tianjin East China Chemicals Co. Ltd.) were used for experiments reported in this paper.

2.2 The experimental process

7075 Al alloy sheets were polished with 500#, 800# and 1500# emery papers in turn, and then cleaned with acetone and ethanol in an ultrasonic bath for 10 min respectively. The samples with different morphology were irradiated by fiber laser for two times with the irradiated area of 10 mm×10 mm, the parameters employed of which: 50 W average power, 20 kHz repetition rate, 200 ns pulse duration, 500 mm/s scanning speed, after desirable patterns of the surface morphology were successfully designed by computer. Afterwards the samples were cleaned with acetone and ethanol in an ultrasonic bath for 15 min respectively. Finally, all of the samples were modified with the 0.01 mol/L solution of stearic acid (SA) at ambient temperature for 60 min and dried in atmosphere condition.

2.3 Characterization

The surface morphologies was analyzed by scanning electron microscopy (SEM, EVO 18, ZEISS), and the surface composition was detected by X-ray photoelectron spectroscopy (XPS, SPECS XR50, Japan). The surface wetting behaviors is assessed by the water contact angle (CA) which is collected by a contact angle meter (JC2000A Powereach, China) with sessile drop method at ambient temperature of 23±2 °C and the relative humidity of 53±5%. Water droplets with the volume of 3 μL were carefully dropped onto the surfaces in five different positions to obtain the average static contact angle value. The infrared spectrum of the samples were recorded with a Fourier Transform-Infrared (FTIR, JACSCO, Japan) spectrometer at a resolution of 2 cm^{-1}. FT-IR spectrum of the samples were obtained between 4,000 and 400 cm^{-1} by an FT-IR spectrometer.

2.4 Anti-icing property

An apparatus composed of temperature control system, image acquisition system and data collection system was established including a Recycled Water Temperature Controller (CMX-250-4/240-NM, OMEGA, America), (TES1310, ESM, China), data acquisition (DAQ11625, Quatronix, China), a CCD camera (73X11H, Mintron, China)and a computer etc. The schematic diagram of the apparatus is shown in Fig.1. Firstly, the sample was fixed with heat conductive silicone grease on the experimental plate horizontally at ambient temperature of 16±2 °C and the relative humidity of 53±5%. And then the temperature of experimental plate, monitored by the digital temperature measuring instrument, was decreased from the room temperature of 16.0 °C to -15 °C at the rate of 0.2°C/s using the Recycled Water Temperature Controller, after the water droplets with the volume of 5 μL were carefully dropped onto the surfaces with different morphology which were fixed on the experimental plate with heat conductive silicone grease, respectively. At the meantime, the icing process was monitored and collected by the CCD camera. Finally, the SHS of the samples, respectively, were tilted with an angle of 5° and fixed on the experimental plate with heat conductive silicone grease as well. When the temperature of the experimental plate was stable at −15 °C, a steam of water was sprayed onto the as-prepared surfaces, and different liquid states were captured by camera.

3. Results and discussion

3.1 Surface morphology

Surface morphology is an important factor of super-hydrophobic properties, therefore, as-prepared surfaces were characterized by SEM. Fig. 2 shows the SEM images of the sample surfaces with different morphology. It can be found that micro scale structure was successfully obtained on 7075 Al alloy substrates, which was proved to play a major role to the different properties of the surfaces. After laser processing, the target part of the surface was removed by high power laser beam, so that the regular morphology was formed as we designed. As shown in Fig.2a, an orderly matrix of regular round humps (R-surface) can be obviously observed in low magnification, as well as the gaps irradiated by laser beam. In high magnification, it is amazing to find the round hump is covered by nano-scale mastoid structure, as shown in Fig.2d, which can attribute to the deposition of SA film. It is easy to deposition on the sharp edge of each hump, and condensate gradually to form the nano-scale mastoid structure on it. This phenomenon is also found in the SEM image of the other two surfaces. In Fig.2b, SEM image of the morphology of the regular square protuberance (S-surface) was captured in low magnification. The distance of each two square protuberances are as same as the round humps` shown in Fig.2a, so that other interference factors except the morphology can be neglected. In the corresponding image, Fig.2e, is the high magnification image of the square protuberance, on which nano-scale mastoid structure is clearly found as well. As to Fig.2c, the image of an array of strips in low magnification are captured by the SEM, while a mountain range-like structure (M-surface) detected in high magnification, as shown in Fig.2f. More importantly, the micro array structure is more complex than the other two as-prepared surfaces. As a result, much more air can be trapped in the void, which is one of the most important character contributing to the water repelling property of superhydrophobic surface.

3.2 Chemical characterization

In addition, FT-IR spectrum was employed to verify the chemical composition of the as-prepared surface modified by stearic acid. It can be seen in Fig.3. That many absorption bands are detected on as-prepared surfaces, compared with the typical FT-IR spectrum of stearic acid, which indicates that 7075 Al alloy aluminum alloy surface has been modified by stearic acid. An absorption peak is found at 1701 cm^{-1} in the low region, corresponding to the free -COO- groups in the typical FT-IR (1702 cm^{-1}) spectrum. This can be attributed to double molecular association of the carboxylic acid molecule. In addition, another two adsorption peaks was found at approximately 2920 cm^{-1} and 2851 cm^{-1} in the high-frequency region respectively, which may be attributed to the -CH_2- asymmetric and symmetric stretching vibrations, while the typical FT-IR spectrum of stearic acid for -CH_2- is at 2917 $cm^{-1}$and 2849 cm^{-1}. Meanwhile, the peak at 1430 cm^{-1} is ascribed to the vibration of the C-O group.

The presence of C, O and Al on the aluminum alloy surfaces modified by stearic acid was revealed by X-ray photoelectron spectroscopy (XPS) investigations, as shown in Fig.4. Fig.4a shows the full-spectrum of the as-prepared surfaces and three strong peaks of Al 2p, C 1s and O 1s were proved to increase significantly compared to the untreated 7075 Al alloy surface, and Fig.2b presents the strong peak of C 1s is at 284.71 eV. In conclusion, as-prepared surfaces were modified by stearic acid successfully, i.e. the existence of C-H and COO- from stearic acid ($CH_3(CH_2)_{16}COOH$) on aluminum alloy surfaces. Low energy materials with micro-structured films make the Cassie state more stable, which will help to amplify the hydrophobicity of the rough substrate. These results allowed us to hypothesize that the bonds between the SA molecules and the metal surface are formed through the condensation reaction, in which the carboxyl group (COO-H) combines with the aluminum hydroxyl group (Al-OH), releasing water and forming the aluminum carboxylate bond COO-Al:**[30-32]**

$$RCOO\text{-}H + H\text{-}O\text{-}Al \rightarrow RCOO\text{-}Al + H_2O$$

3.3 Wettability

The topographical structure and the chemical compositions are two important factors determined the wettability of the solid material.[33-36] As we mention above, all of the as-prepared superhydrophobic surfaces were successfully covered with a film of SA molecules. Once morphology of as-prepared surfaces changed from smooth to a topological rough structure, the wettability of the surfaces transformed from a hydrophilic character to a superhydrophobic state. Fig.5 shows the water contact angle (WCA) of the as-prepared surfaces with different morphology, bare surface(B), square protuberance structure (S), round hump structure (R) and mountain range-like structure (M), modified by stearic acid. The bare surface without any structure and SA coating exhibits the hydrophility with contact angle of 53°. The surface of mountain range-like structure shows an excellent superhydrophobicity, and the WCA reached 166±2°. Although the WCA of the other two surfaces, surface of square protuberance structure and surface of round hump structure, are not as high as the surface of mountain range-like structure, they are shown the superhydrophobic property as well, reaching 157±2.8° and 161±2.2°. As proved by many researches, the morphology of the surface is an indispensable factor to superhydrophobic property, thus the optimum micro-structure of the surface is made, the better superhydrophobic surface is obtained. The insets of Fig.5 systematically illustrates the state of as-prepared surfaces, labelled as INS.a, b and c respectively. INS.a shows the model of water droplet on bare surface, which can be recognized as Wenzel state. At this state, the wet contact (i.e., whole contact) between solid–liquid interfaces, so the existed continuous three-phase contact line leads to high adhesion of the surface, for which drop can hardly rolls off the surface. INS.b and c are models of the other three as-prepared superhydrophobic surfaces, which can be recognized as Cassie–Baxter state. Compared with the bare surface, the droplets are of composite contact on solid–liquid interfaces, so the discontinuous three-phase contact line exists and leads to low adhesion of the surface, for which drop easily rolls off the surface. More importantly, with so much trapped-air between the droplets and surfaces, the droplet is completely suspended over the surfaces, which contributes the different wettability of the surfaces. However, the triple-phrase contact line of different superhydrophobic surfaces is not identical. Superhydrophobic surfaces with square protuberance structure and round hump structure (as shown in the INS.b) have larger contact area than surfaces with mountain range-like structure (as shown in INS.c), so this could attribute to the difference of icing time.

3.4 Anti-icing properties

Superhydrophobic surfaces, as a passive anti-icing surfaces, has shown a promising future in the industrial applications, and great efforts have been made to invent new patent of these material with anti-icing and deicing capacities and study the mechanism.[6, 37] Because of the existence of vapor pockets at the solid-liquid interface in the Cassie-Baxter state[38], water droplet can be suspended over the superhydrophobic surfaces and easily roll off. The delayed freezing time of water droplet on the superhydrophobic surface is another important indicator for the anti-icing property. [39-42] As discussed above, the as-prepared structured surface shows various wetting properties, which may really affect anti-icing properties under low temperature conditions. Fig.6 (1)a, b, c and d show the real-time status of water droplet in the volume of 5 μL on the as-prepared surface of mountain range-like structure (M), square protuberance structure (S), round hump structure (R) and bare surface(B) respectively. Initially, the reference drops on all surfaces are transparent. When the temperature of the experimental plate is decreased gradually, the drop on the B-surface becomes non-transparent at first after 319s, which indicates the drop is becoming frozen. However, the shape of the drops is changed after 325s, indicating the drop is frozen totally. Observed in turn, the drop on the R-surface and S-surface becomes non-transparent after 1146 s and 1160s respectively, and frozen after 1153s and 1165s respectively with shape being changed. Obviously, the drop on the M-surface then becomes non-transparent after 1933s, and is frozen after 1938s, indicating this surface has a relatively long time to resist the water freezing. To further illustrate the icing process, Fig. 6e shows the icing mechanism of water droplet on as-prepared superhydrophobic surfaces. As the temperature of experimental plate decreased and stably kept at -15°C with the relative humidity of 53±5%, the Cassie–Baxter state still existed on the superhydrophobic surfaces. But when delay time is at 1146s, droplet on R-surfaces became non transparent firstly, and shape of the droplet was changed to peach-like at 1154s. At that time, Cassie–Baxter state missed and droplet was not suspended at all. However, when the temperature of the experimental plate return to ambient temperature, the SHS recovered to Cassie–Baxter state, and droplet return to be suspended as well. All superhydrophobic surfaces mentioned above share with the same mechanism. As to B-surface, droplets exist as hemisphere, which can be described as Wenzel state[43].

Consequently, delayed freezing time is roughly recorded by observing the non-transparency of the drop at -15 °C, as shown in Fig.6(2). The icing time on these SHS can be postponed from 325s to 1938s compared to the normal aluminum alloy surface. This implies that the differences of the micro-structure of SHS can significantly impact delayed freezing time. When the temperature of as-prepared surface was heated to room temperature, the droplet returns to be suspended upwards and the discontinuous three-phase contact line between the droplet and surface is basically recovered, which is slightly similar to the original contact state.

The temperature-induced pinning transition of droplets observed for the SHS at -15 °C can be explained using a model which analyzes droplet heat transfer process at the interface between the droplet and the micro-structure, as illustrated by Fig.6(3)a. Considering the droplet is suspended over the surfaces and the solid–liquid–air three-phase interfaces exists, there are two approaches to gain or lose heat, i.e. it gains heat from air in forms of contact heat conduction and thermal radiation and it loses heat to the cold surface through contact heat conduction and thermal radiation between the drop and the micro-structure. But what we focus on is the process of icing, so we leave out the heat gain by micro-structure for the temperature of experimental plate is lower than that of droplet.

The relationship between heat gain and loss is expressed as:[44]

$$Q_d = Q_g - Q_l - Q_l^*$$

Where Q_d is the heat quantity of droplet in unit time; Q_g is the heat quantity gains through thermal radiation in unit time; Q_l and Q_l^* is heat quantity loses through thermal radiation and heat transfer in unit time.

To further explain the mechanism of heat transfer on SHS, we introduce the area formula of the sphere and the equation of thermal radiation, but some hypotheses have to be made:

(1) The shape of droplet is never changed but a ball;

(2) The thermal radiation between the droplet and air is homogeneous;

The equations involved present as follows:

Equation of irregular sphere surface area;

$$S_d = 2\pi R^2 (1 - \sin\theta) \tag{1}$$

Where S_d is the surface area of sphere; R is the radius of sphere; θ is the spherical center angle;

The heat transfer through conduction between the interface of the water droplet and the coating surface can be described as the following equation:[45]

$$Q = \alpha S_d \left(T_A - T_d\right) \tag{2}$$

Where Q is the heat quantity in unit time; α is radiant heat-transfer coefficient(according to different materials); T_A is the temperature of ambient temperature; T_d is the temperature of sphere.

Referring to the equations mentioned above, we put forward an equation of heat gain and loss:

$$\begin{aligned} Q_d &= \alpha S_g\left(T_A - T_d\right) - \alpha S_l\left(T_A^{\lambda} - T_d\right) - Q_l^{*} \\ &= \alpha \bullet 2\pi R^2\left(1+\sin\beta\right)\left(T_A - T_d\right) - \alpha \bullet 2\pi R^2\left(1-\sin\beta\right)\left(T_A^{\lambda} - T_d\right) - Q_l^{*} \end{aligned}$$

Where S_g is the heat gain surface area of sphere; S_l is the heat loss surface area of sphere; T_A^{λ} is temperature of the air between droplet and experimental plate; β is contact angle of droplet (CA).

What we can learn in the equation is, there are two approaches to keep the heat quantity of droplet in unit time Q_d, increasing the contact angle of droplet and decreasing the heat quantity loses through heat transfer. That means the bigger CA is, the more air trapped under the droplet, so as to the less loss of heat quantity. Thus, this can well explain the difference of delayed freezing times to the as-prepared superhydrophobic surfaces. For example, the large contact angle of M-surface contributes to more air trapped under the droplet, and less liquid–solid contact area on the surface. As to the B-surface, there is no trapped-air under the droplet and large liquid–solid contact area (as shown in Fig. 6(3)b), so the equation of heat gain and loss can be expressed as follows:[44]

$$Q_d = Q_g - Q_l^{*}$$

Obviously, heat loss in unit time through heat transfer of liquid-solid interface is larger than heat gain in unit time through thermal radiation. Consequently, the heat quality of droplet decreases soon, leading to short delayed freezing times.

For further tests to the anti-icing property of as-prepared surfaces, with the relative humidity of 53±5%, a stream of water was sprayed onto the B-, R-, S- and M-surfaces with an angle of 5°, respectively, the temperature of which was controlled at -15 ºC stably, for 5 min in a permanent speed. Final result of the test is shown in Fig.7. In Fig.7a, the iced area was separated by red lines on S-surface. Almost 40% of the experimental area separated by blue square was covered with a thin film of ice, while most of the experimental area still exhibits ice-free properties. As to R-surface (Fig.9b), there are some droplets, separated by red circles, sticking on the experimental area, 30% of which was covered by a big block of ice separated by red lines. Obviously, M-surfaces (Fig.7c) shows the best anti-icing property, on which only some droplets stuck within experimental area, a large block of ice, however, was found on the non-experimental area. Moreover, in contrast to SHS, a strip of ice was clearly found on B-surface separated by red lines, shown in Fig.7d. As we discussed above, SHS exhibit an excellent water-repelling property at ambient temperature, as well as low adhesion. However, the situation is different, as the temperature decrease to -15ºC. To well illustrate this phenomenon, we establish a model of icing process to schematically illustrate the mechanism of dynamic situation, as shown in Fig.8. It has been proved that droplets can be suspended over the SHS, resulting from the existence of trapped-air in the micro-structure and low-surface-energy material on the surface. However, the micro water droplets are easy to condensate in the gaps on the surface of micro-structure at low temperature.[46] In addition, some discrete frozen micro-drops first appeared on the superhydrophobic surfaces, and the following icing mainly occurred on these microcrystals and then expanded around them until covering the entire surface.[47] As a result, the Cassie–Baxter state disappears gradually, for most of the place used to trap air is taken up by condensate water. With the temperature of experimental plate decreased further, the surfaces adhesion strength increased dramatically.[48, 49] Once the strength is larger than Van Der Waals force existing between the water molecules, the bottom layer of water could be peeled off and left on the surface other than flow down, even though the up layer is still flowing. Finally, ice accumulation occurs on the superhydrophobic surfaces.

Conclusions

In summary, we have studied the anti-icing property of three different superhydrophobic surfaces, based on substrates of 7075 Al alloy, with different morphology, i.e. round hump, square protuberance and mountain-range-like structure, prepared by laser processing. Firstly, the wettability of the as-prepared surfaces have been studied at ambient temperature with the relative humidity of 53 ± 5%, and the SHS of mountain-range-like structure shows the best superhydrophobic property with a contact angle of 166 ± 2°. Furthermore, systematic investigations of the static and dynamic freezing process show that the anti-icing capability is significantly impacted by the micro-structure of these superhydrophobic surfaces. Compared with the bare 7075 Al alloy, the SHS of mountain-range-like structure owns the longest delay time of 1938s in static situation and the best ice-free property in dynamic situation. More importantly, we introduced a model to analyze heat transfer process between the droplet and the structured surfaces. This study offers an insight into understanding the heat transfer process of the superhydrophobic surface, so as to further research about its unique property against ice accumulation.

ACKNOWLEDGEMENTS

The authors thank the National Natural Science Foundation of China (Nos. 51275555, 51475200 and 51325501), Science and Technology Development Project of Jilin Province (No.20150519007JH) and 111 project (B16020) of China.

References

[1] J.L. Laforte, M.A. Allaire, J. Laflamme, State-of-the-art on power line de-icing, Atmos. Res., 46 (1998) 143-158.

[2] O. Parent, A. Ilinca, Anti-icing and de-icing techniques for wind turbines: Critical review, Cold Reg. Sci. Technol., 65 (2011) 88-96.

[3] S.A. Kulinich, M. Farzaneh, Ice adhesion on super-hydrophobic surfaces, Appl. Surf. Sci., 255 (2009) 8153-8157.

[4] Z. Zuo, R. Liao, C. Guo, Y. Yuan, X. Zhao, A. Zhuang, Y. Zhang, Fabrication and anti-icing property of coral-like superhydrophobic aluminum surface, Appl. Surf. Sci., 331 (2015) 132-139.

[5] M. Jung, T. Kim, H. Kim, R. Shin, J. Lee, J. Lee, J. Lee, S. Kang, Design and fabrication of a large-area superhydrophobic metal surface with anti-icing properties engineered using a top-down approach, Appl. Surf. Sci., 351 (2015) 920-926.

[6] J. Lv, Y. Song, L. Jiang, J. Wang, Bio-inspired strategies for anti-icing, ACS nano, 8 (2014) 3152-3169.

[7] S.A. Kulinich, M. Farzaneh, How wetting hysteresis influences ice adhesion strength on superhydrophobic surfaces, Langmuir, 25 (2009) 8854-8856.

[8] L. Feng, Y. Zhang, J. Xi, Y. Zhu, N. Wang, F. Xia, L. Jiang, Petal Effect: A Superhydrophobic State with High Adhesive Force, Langmuir, 24 (2008) 4114-4119.

[9] X.-Q. Feng, X. Gao, Z. Wu, L. Jiang, Q.-S. Zheng, Superior Water Repellency of Water Strider Legs with Hierarchical Structures: Experiments and Analysis, Langmuir, 23 (2007) 4892-4896.

[10] Y. Zheng, X. Gao, L. Jiang, Directional adhesion of superhydrophobic butterfly wings, Soft Matter, 3 (2007) 178-182.

[11] T. Sun, L. Feng, X. Gao, L. Jiang, Bioinspired Surfaces with Special Wettability, Accounts Chem. Res., 38 (2005) 644-652.

[12] N. Gao, Y.Y. Yan, X.Y. Chen, X.F. Zheng, Superhydrophobic Composite Films Based on THS and Nanoparticles, J. Bionic Eng., 7 (2010) S59-S66.

[13] H.A. Stone, Ice-Phobic Surfaces That Are Wet, ACS Nano, 6 (2012) 6536-6540.

[14] C. Dorrer, J. Rühe, Some thoughts on superhydrophobic wetting, Soft Matter, 5 (2009) 51-61.

[15] A. Marmur, Wetting on Hydrophobic Rough Surfaces: To Be Heterogeneous or Not To Be?, Langmuir, 19 (2003) 8343-8348.

[16] Y. Liu, Y. Bai, J. Jin, L. Tian, Z. Han, L. Ren, Facile fabrication of biomimetic superhydrophobic surface with anti-frosting on stainless steel substrate, Appl. Surf. Sci., 355 (2015) 1238-1244.

[17] D.K. Sarkar, M. Farzaneh, R.W. Paynter, Wetting and superhydrophobic properties of PECVD grown hydrocarbon and fluorinated-hydrocarbon coatings, Appl. Surf. Sci., 256 (2010) 3698-3701.

[18] L. Cao, A.K. Jones, V.K. Sikka, J. Wu, D. Gao, Anti-icing superhydrophobic coatings, Langmuir, 25 (2009) 12444-12448.

[19] P. Guo, Y. Zheng, M. Wen, C. Song, Y. Lin, L. Jiang, Icephobic/anti-icing properties of micro/nanostructured surfaces, Adv. Mater., 24 (2012) 2642-2648.

[20] P. Kim, T.-S. Wong, J. Alvarenga, M.J. Kreder, W.E. Adorno-Martinez, J. Aizenberg, Liquid-Infused Nanostructured Surfaces with Extreme Anti-Ice and Anti-Frost Performance, ACS Nano, 6 (2012) 6569-6577.

[21] J.D. Brassard, D.K. Sarkar, J. Perron, Synthesis of monodisperse fluorinated silica nanoparticles and their superhydrophobic thin films, ACS Appl. Mater. Interfaces, 3 (2011) 3583-3588.

[22] N. Puretskiy, J. Chanda, G. Stoychev, A. Synytska, L. Ionov, Anti-Icing Superhydrophobic Surfaces Based on Core-Shell Fossil Particles, Adv. Mater. Interfaces, 2 (2015) n/a-n/a.
[23] M. Zou, S. Beckford, R. Wei, C. Ellis, G. Hatton, M.A. Miller, Effects of surface roughness and energy on ice adhesion strength, Appl. Surf. Sci., 257 (2011) 3786-3792.
[24] J. Liu, H. Guo, B. Zhang, S. Qiao, M. Shao, X. Zhang, X.Q. Feng, Q. Li, Y. Song, L. Jiang, J. Wang, Guided Self-Propelled Leaping of Droplets on a Micro-Anisotropic Superhydrophobic Surface, Angew. Chem. Int. Ed. Engl., 55 (2016) 4265-4269.
[25] K. Rykaczewski, J.H.J. Scott, S. Rajauria, J. Chinn, A.M. Chinn, W. Jones, Three dimensional aspects of droplet coalescence during dropwise condensation on superhydrophobic surfaces, Soft Matter, 7 (2011) 8749-8752.
[26] M. He, X. Zhou, X. Zeng, D. Cui, Q. Zhang, J. Chen, H. Li, J. Wang, Z. Cao, Y. Song, L. Jiang, Hierarchically structured porous aluminum surfaces for high-efficient removal of condensed water, Soft Matter, 8 (2012) 6680.
[27] Q. Zhang, M. He, J. Chen, J. Wang, Y. Song, L. Jiang, Anti-icing surfaces based on enhanced self-propelled jumping of condensed water microdroplets, Chem. Commun., 49 (2013) 4516-4518.
[28] S.W. Kim, D.Y. Kim, W.G. Kim, K.D. Woo, The study on characteristics of heat treatment of the direct squeeze cast 7075 wrought Al alloy, Mater. Sci. Eng. A, 304–306 (2001) 721-726.
[29] R.K. Bhushan, S. Kumar, S. Das, Effect of machining parameters on surface roughness and tool wear for 7075 Al alloy SiC composite, Int. J. Adv. Manuf. Technol., 50 (2010) 459-469.
[30] S.A. Kulinich, M. Honda, A.L. Zhu, A.G. Rozhin, X.W. Du, The icephobic performance of alkyl-grafted aluminum surfaces, Soft Matter, 11 (2015) 856-861.
[31] X. Yao, Q. Chen, L. Xu, Q. Li, Y. Song, X. Gao, D. Quéré, L. Jiang, Bioinspired Ribbed Nanoneedles with Robust Superhydrophobicity, Adv. Funct. Mater., 20 (2010) 656-662.
[32] B. Somlo, V. Gupta, A hydrophobic self-assembled monolayer with improved adhesion to aluminum for deicing application, Mech. Mater., 33 (2001) 471-480.
[33] J. Zhang, Y. Han, A Topography/Chemical Composition Gradient Polystyrene Surface: Toward the Investigation of the Relationship between Surface Wettability and Surface Structure and Chemical Composition, Langmuir, 24 (2008) 796-801.
[34] N. Takeshita, L.A. Paradis, D. Öner, T.J. McCarthy, W. Chen, Simultaneous Tailoring of Surface Topography and Chemical Structure for Controlled Wettability, Langmuir, 20 (2004) 8131-8136.
[35] Q. Fu, G.V. Rama Rao, S.B. Basame, D.J. Keller, K. Artyushkova, J.E. Fulghum, G.P. López, Reversible Control of Free Energy and Topography of Nanostructured Surfaces, J. Am. Chem. Soc., 126 (2004) 8904-8905.
[36] D. Öner, T.J. McCarthy, Ultrahydrophobic Surfaces. Effects of Topography Length Scales on Wettability, Langmuir, 16 (2000) 7777-7782.

[37] M.J. Kreder, J. Alvarenga, P. Kim, J. Aizenberg, Design of anti-icing surfaces: smooth, textured or slippery?, Nat. Rev. Mater., 1 (2016) 15003.
[38] A. Cassie, S. Baxter, Wettability of porous surfaces, Trans. Faraday Soc., 40 (1944) 546-551.
[39] G. Heydari, E. Thormann, M. Järn, E. Tyrode, P.M. Claesson, Hydrophobic Surfaces: Topography Effects on Wetting by Supercooled Water and Freezing Delay, J. Phys. Chem. C, 117 (2013) 21752-21762.
[40] J. Hu, K. Xu, Y. Wu, B. Lan, X. Jiang, L. Shu, The freezing process of continuously sprayed water droplets on the superhydrophobic silicone acrylate resin coating surface, Appl. Surf. Sci., 317 (2014) 534-544.
[41] F. Arianpour, M. Farzaneh, S.A. Kulinich, Hydrophobic and ice-retarding properties of doped silicone rubber coatings, Appl. Surf. Sci., 265 (2013) 546-552.
[42] L. Boinovich, A.M. Emelyanenko, V.V. Korolev, A.S. Pashinin, Effect of wettability on sessile drop freezing: when superhydrophobicity stimulates an extreme freezing delay, Langmuir, 30 (2014) 1659-1668.
[43] R.N. Wenzel, Resistance of solid surfaces to wetting by water, Ind. Eng. Chem., 28 (1936) 988-994.
[44] X. Zhan, Y. Yan, Q. Zhang, F. Chen, A novel superhydrophobic hybrid nanocomposite material prepared by surface-initiated AGET ATRP and its anti-icing properties, J. Mater. Chem. A, 2 (2014) 9390-9399.
[45] Y. Tang, Q. Zhang, X. Zhan, F. Chen, Superhydrophobic and anti-icing properties at overcooled temperature of a fluorinated hybrid surface prepared via a sol-gel process, Soft Matter, 11 (2015) 4540-4550.
[46] M. Wen, L. Wang, M. Zhang, L. Jiang, Y. Zheng, Antifogging and icing-delay properties of composite micro- and nanostructured surfaces, ACS Appl. Mater. Interfaces, 6 (2014) 3963-3968.
[47] Q. Hao, Y. Pang, Y. Zhao, J. Zhang, J. Feng, S. Yao, Mechanism of delayed frost growth on superhydrophobic surfaces with jumping condensates: more than interdrop freezing, Langmuir, 30 (2014) 15416-15422.
[48] S.A. Kulinich, M. Farzaneh, On ice-releasing properties of rough hydrophobic coatings, Cold Reg. Sci. Technol., 65 (2011) 60-64.
[49] L.B. Boinovich, A.M. Emelyanenko, Anti-icing Potential of Superhydrophobic Coatings, Mendeleev Commun., 23 (2013) 3-10.

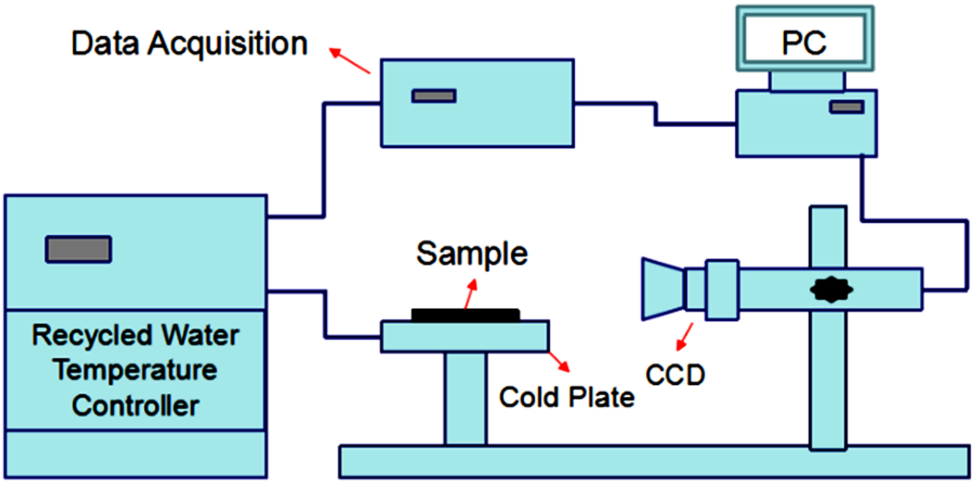

Fig.1 The schematic representation of the experimental setup.

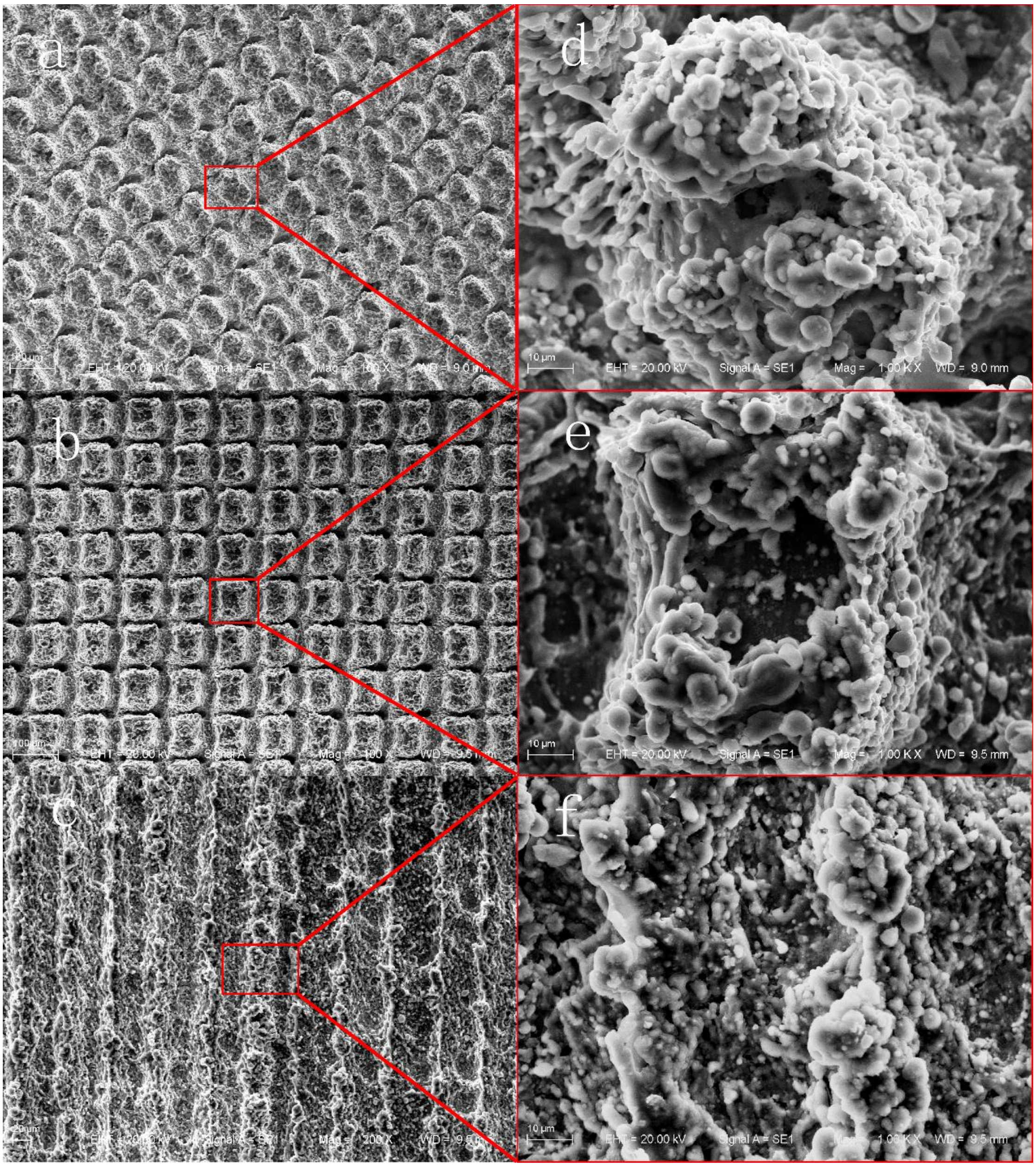

Fig.2 SEM images of the sample surfaces with different morphology: (a) Surface with the morphology of the regular round humps(R-surface), (b) Surface with morphology of the regular square protuberance(S-surface), (c) Surface with the morphology of mountain range-like structure (M-surface), (d-f) high magnification SEM image of the corresponding structured surfaces, respectively.

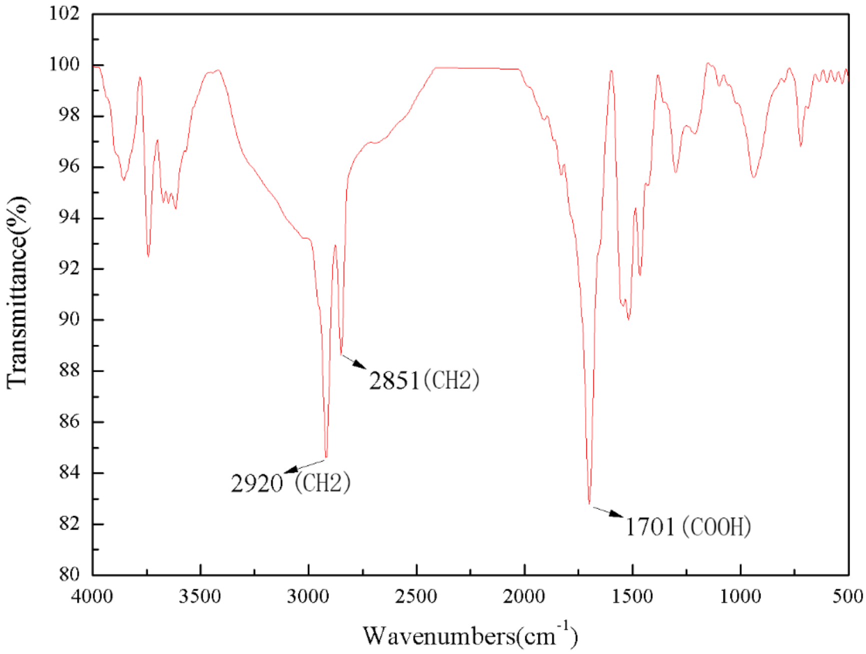

Fig.3 FT-IR spectrum of the Aluminum alloy surfaces modified by stearic acid.

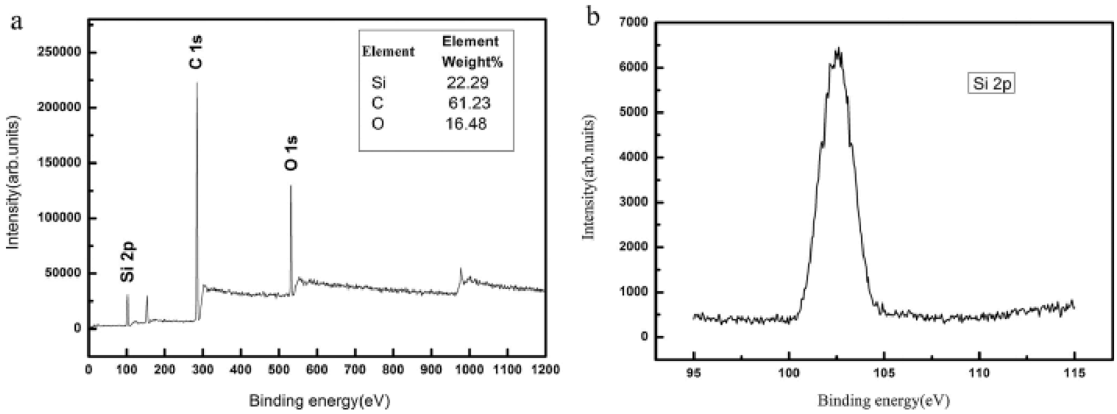

Fig.4 XPS spectra of the as-prepared superhydrophobic aluminum alloy surface of (a) full-spectrum and (b) C 1s.

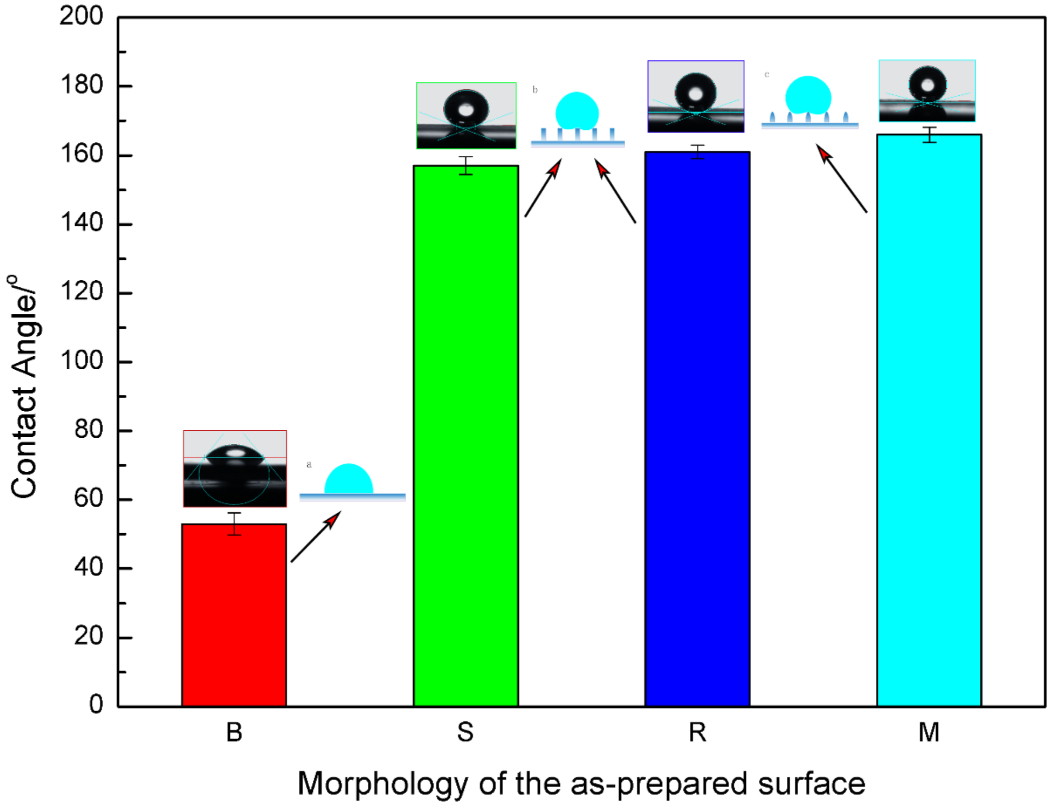

Fig.5 WCA of different morphology of the as-prepared surface, bare surface(B) ,square protuberance structure (S),round hump structure (R) and mountain range-like structure (M),insets are optical images of the static contact angle of 3 μL water droplets. Insets are schematic illustration of the wettability on the as-prepared surface with different morphology; the triple-phrase contact line of different superhydrophobic surfaces is not identical, superhydrophobic surfaces with square protuberance structure and round hump structure have larger contact area than surfaces with mountain range-like structure.

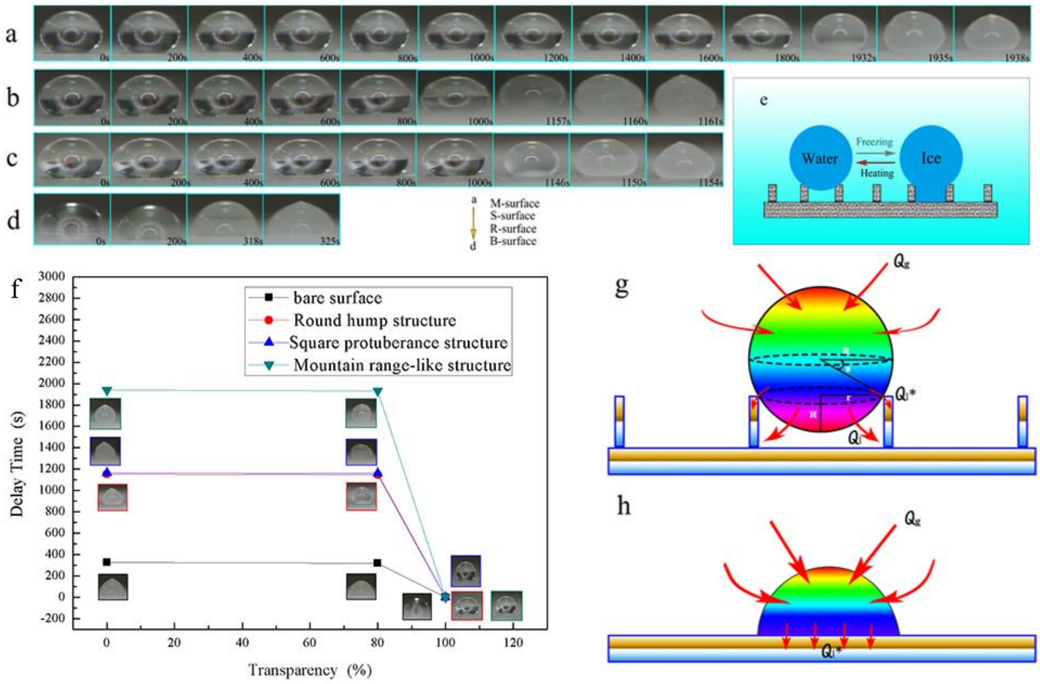

Fig.6 (1) In situ observation of ice formation on B-, R-, S-, and M-surfaces at –15 ºC (a-d), (e) icing mechanism of water droplet on as-prepared superhydrophobic surfaces. (2) Delayed freezing times of ice formation on B-, R-, S- and M-surfaces at –15 ºC, and insets are the status of water droplet at different time. (3) Model of heat transfer process at the interface between the droplet and surface, (a) superhydrophobic surface, (b) bare surface.

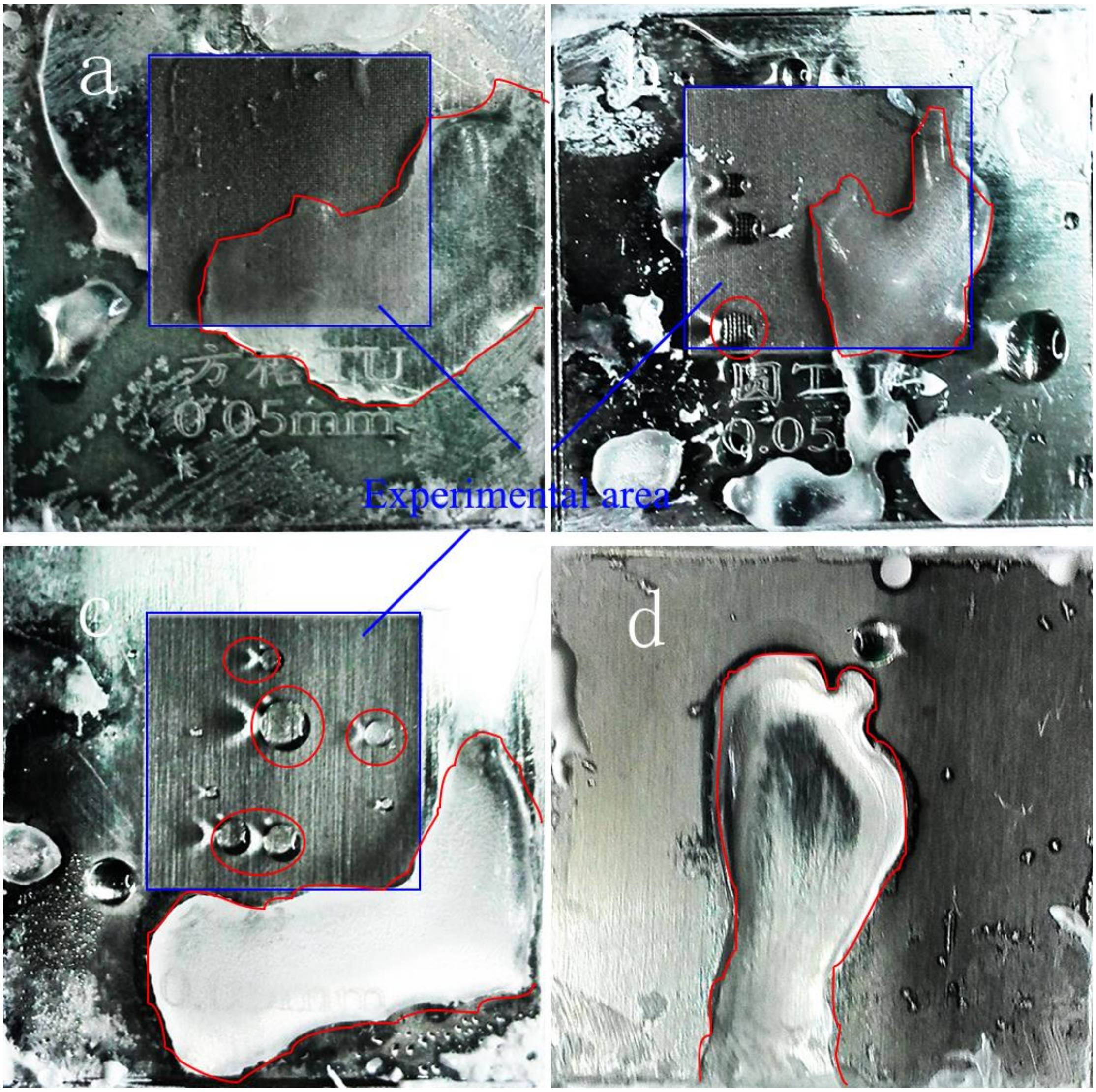

Fig.7 The photographs of anti-icing test by spraying a stream of water onto the as-prepared surfaces(a-d) square protuberance structure (S),round hump structure (R) and mountain range-like structure (M) and bare surface(B) respectively, the temperature of which was controlled at -15 °C stably.

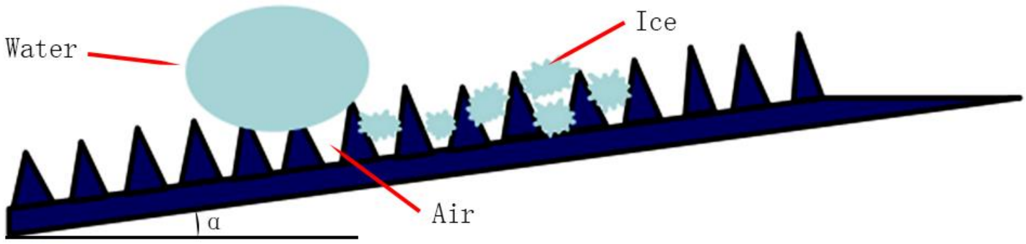

Fig.8 Icing process model for dynamic situation. The micro water droplets are easy to condensate in the gaps on the surface of micro-structure at low temperature. As a result, most of the place used to trap air is taken up by condensate water, so that the Cassie–Baxter state disappears gradually. With the temperature of experimental plate decreased further, parts of water could be peeled off and left on the surface other than flow down, when the adhesive force is larger than Van Der Waals force of the water.